

Investigation of the performance of an optimised MicroCAT, a GEM and their combination by simulations and current measurements [★]

A. Orthen ^{a,*}, H. Wagner ^a, H.J. Besch ^a, R.H. Menk ^b,
A.H. Walenta ^a, U. Werthenbach ^a

^a*Universität Siegen, Fachbereich Physik, Emmy-Noether-Campus, Walter-Flex-Str. 3, 57068 Siegen, Germany*

^b*ELETTRA, Sincrotrone Trieste, S.S. 14, km 163.5, Basovizza, 34012 Trieste, Italy*

Abstract

A MicroCAT (Micro Compteur à Trous) structure which is used for avalanche charge multiplication in gas filled radiation detectors has been optimised with respect to maximum electron transparency and minimum ion feedback. We report on the charge transfer behaviour and the achievable gas gain of this device. A three-dimensional electron and ion transfer simulation is compared to results derived from electric current measurements. Similarly, we present studies of the charge transfer behaviour of a GEM (Gas Electron Multiplier) by current measurements and simulations. Finally, we investigate the combination of the MicroCAT and the GEM by measurements with respect to the performance at different voltage settings, gas mixtures and gas pressures.

PACS: 02.60.Cb; 51.10.+y; 51.50.+v; 29.40.Cs

Key words: Micro pattern gaseous detectors; Gas gain devices; GEM; Gas electron multiplier; MicroCAT; Gas gain; Charge transfer; Electron transparency; Ion feedback

[★] Work supported by the European Community (contract no. ERBFMGECT980104).

* Corresponding author. Tel.: +49 271-740-3563; fax: +49 271-740-3533; e-mail: orthen@alwa02.physik.uni-siegen.de.

1 Introduction

With the rise of micropattern gas gain devices like GEM [1], MICROMEAS [2], CAT [3] or MicroCAT [4] the field of application of gas filled detectors has been widened up. These structures accept high rates and due to their parallel plate geometry they produce short signals and good time-resolution.

Several attempts have been made in the past to enhance the gain and the reliability by combining micropattern structures. The performance of the combination of MSGCs with GEM structures is reported in Refs. [5,6,7]. The combinations of MSGCs and MGCs with GEM, MICROMEAS and Plate Avalanche Chambers are discussed in Ref. [8] with a special emphasis on rate and gain limitations. A GEM, used as a preamplification stage, has also been successfully combined with a Groove Chamber [9]. First results of a device combining a MICROMEAS and a GEM have been presented in Ref. [10]. GEM structures have been combined to double GEM [11], triple GEM and even to quad GEM configurations [12,13], which reach an enormous gas gain in the order of $10^5 - 10^6$.

Adding a GEM to the MicroCAT structure a stable operation with respect to sparks is obtained at moderate potentials; nevertheless quite high gas gains are achievable at higher potentials. For this reason the detector can be operated in applications where higher gas pressures (≈ 3 bar) and high- Z gases (like e.g. Xenon) are required, i.e. in X-ray detection, as will be shown in this paper.

The intention of this investigation is to optimise MicroCAT- and GEM-based detector systems for X-ray imaging (typical photon energy range: 5 – 25 keV), where the drift gaps are usually several cm large and the drift fields are in the range of 1 kV/cm or even less.

2 Study of the optimised MCAT215

In the past several MicroCAT structures have been investigated [4]. Recently, an optimised MicroCAT mesh has been produced by Stork Screens¹. In this section we compare the charge transfer derived from current measurements to simulations, and we demonstrate that the new device is superior to previously investigated MicroCAT structures with respect to maximum electron transparency (to maximise the effective gain) and minimum ion feedback (to avoid field perturbations in the drift region).

¹ Stork Screens, Boxmeer, Netherlands

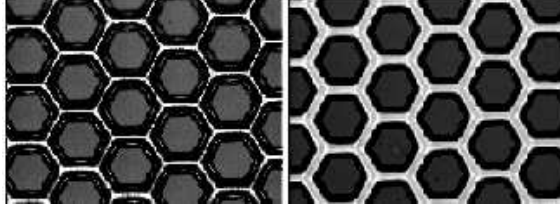


Fig. 1. Microscopic photography of both sides of the optimised MicroCAT structure.

type	holes/inch	pitch l	hole diameter h	open area	thickness
MCAT155	155	$164 \mu\text{m}$	$116 \mu\text{m}$	45.4 %	$70 \mu\text{m}$
MCAT215	215	$118 \mu\text{m}$	$79 \mu\text{m}$	40.6 %	$55 \mu\text{m}$
MCAT305	305	$83 \mu\text{m}$	$45 \mu\text{m}$	26.5 %	$55 \mu\text{m}$
Opt. MCAT215	215	$118 \mu\text{m}$	$78 \mu\text{m}$	39.5 %	$25 \mu\text{m}$

Table 1

Dimensions of the MicroCAT structures.

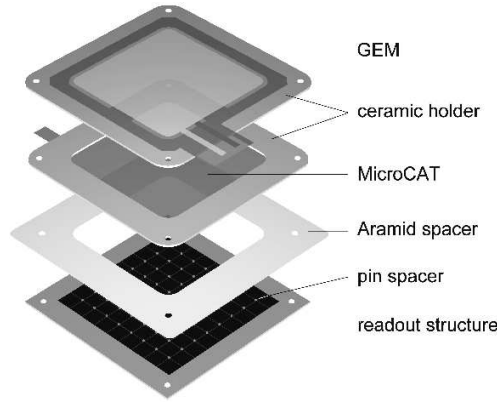


Fig. 2. Schematic view of the detector setup. The distance between the GEM and the MicroCAT amounts to 2 mm. The drift cathode is mounted at a distance of 25 mm above the GEM structure.

2.1 Characteristics

The MicroCAT structure (see Fig. 1) has been optimised with respect to maximum electron transparency and minimum ion feedback while retaining a good mechanical stability [14]. The parameters of the newly built device are given together with those of previously used MicroCATs in Table 1. The holes which have a hexagonal shape with edges rounded by the production process form a hexagonal lattice. The cathode distance between the MicroCAT and the subjacent anode amounts to $d = (130 \pm 10) \mu\text{m}$ (see Fig. 2), which is in fact very close to the optimum distance of about $100 \mu\text{m}$ with respect to maximum time-resolution. The anode is realised by an interpolating resistive readout structure [15,16]. The drift region has a height of 27 mm (since the

GEM structure is not mounted). For all measurements in this section the detector volume is filled with a gas mixture of 1 bar Ar/CO₂ (90/10).

The charge transfer behaviour of the MicroCAT depends only on the ratio $\eta = E_{\text{drift}}/E_{\text{MCAT}}$ of the fields above and below the mesh. This has been confirmed by simulations [14].

2.2 Charge transfer behaviour

For the determination of the charge transfer the measurement of at least two of the following three currents is necessary:

$$I_{\text{drift}} = I_0 + \delta \cdot \varepsilon \cdot (G - 1) \cdot I_0 \quad (1)$$

$$I_{\text{MCAT}} = -(1 - \varepsilon) \cdot I_0 + (1 - \delta) \cdot \varepsilon \cdot (G - 1) \cdot I_0 \quad (2)$$

$$I_{\text{anode}} = -\varepsilon \cdot G \cdot I_0 \quad (3)$$

with I_0 as the incoming current:

$$I_0 = R \cdot \frac{E_\gamma}{W} \cdot e. \quad (4)$$

Here, ε denotes the electron transparency, δ the ion feedback, which describes the fraction of ions drifting back to the drift cathode, G the gas gain, R the photon rate, E_γ the mean energy deposited by the photons in the detector, W the mean ionisation potential of the gas atoms/molecules and e the elementary charge.

Since Eqs. 1-3 fulfill current conservation, equivalent to $\sum I = 0$, only two of the three relations are independent and thus not sufficient to determine all three unknown variables ε , δ and G . Therefore, one additional condition is required, which we determine by the simulation presented in the following paragraph.

2.2.1 Simulations

The electric fields for the MicroCAT structures have been calculated in three dimensions using the Maxwell package [17]. The charge drift was calculated using the Garfield program [18]. The gas properties used for the Garfield simulation like electron diffusion or drift velocity are calculated by the Magboltz program [19,20]. The distance between the lower side of the MCAT and the anode has been set to 100 μm , the MCAT voltage to -450 V while the anode structure has zero potential, leading to an average electric field in the amplification gap of $E_{\text{MCAT}} = 45$ kV/cm. All potentials are assumed to be constant during the simulation since the change of the potential during one multiplication process due to charge motion in the real detector is calculated to be in

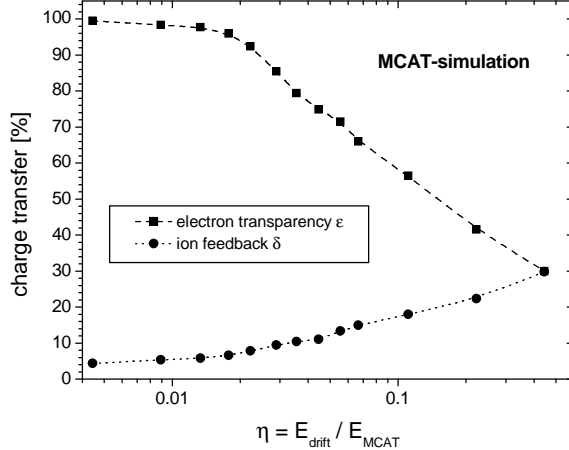


Fig. 3. Simulated electron transparency ε and ion feedback δ for the optimised MCAT215 structure.

the order of $\mathcal{O}(\text{mV})$.

Diffusion has been included for the drifting electrons but neglected for the ions since this contribution is expected to be small. Charge multiplication has not been considered. The ion feedback simulation is based on an effective size of the ion cloud of about $\sigma = 30 \mu\text{m}$. A more detailed description of the charge transfer simulation can be found in Ref. [14].

The results of the simulation for the electron transparency ε and ion feedback δ are shown in Fig. 3 as a function of the ratio $\eta = E_{\text{drift}}/E_{\text{MCAT}}$ for fixed E_{MCAT} . As expected, the ion feedback increases with η but the electron transparency decreases.

2.2.2 Measurements and comparison with simulations

We have measured the electric currents at all electrodes as a function of the ratio $\eta = E_{\text{drift}}/E_{\text{MCAT}}$ with the settings $E_{\text{MCAT}} \approx 49 \text{ kV/cm}$ and $d = 130 \mu\text{m}$. Due to technical reasons the measurements of ε and δ are restricted to small values of η below about 0.03. In Section 4 the range of η is extended to larger values of about 0.16.

From the measured currents we compute the effective gain G_{eff} using the relations 1–3:

$$G_{\text{eff}} = \varepsilon \cdot G = \frac{I_{\text{drift}} + I_{\text{MCAT}}}{I_0}. \quad (5)$$

The gain variation due to the increasing drift field in the investigated range of η has been calculated with Garfield for electrons starting $100 \mu\text{m}$ above the MCAT along the symmetry axis of a hole to be less than 2%. Therefore, the measured product $\varepsilon \cdot G$ is expected to follow the simulation of ε . In Fig. 4 where we compare the measurement with the simulation, we observe that contrary to the simulation the measured product drops at small values of

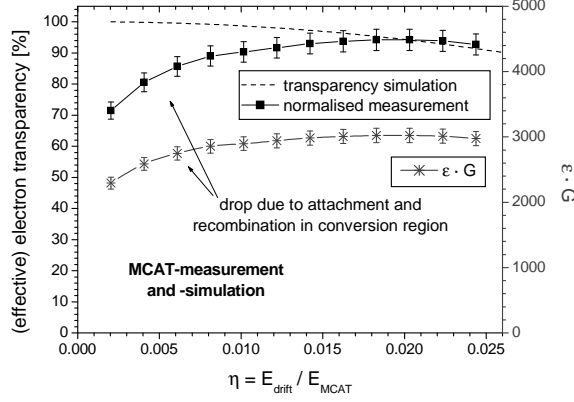


Fig. 4. Measured product $\varepsilon \cdot G$ and comparison of the normalised product with the simulated electron transparency for the optimised MCAT215 structure.

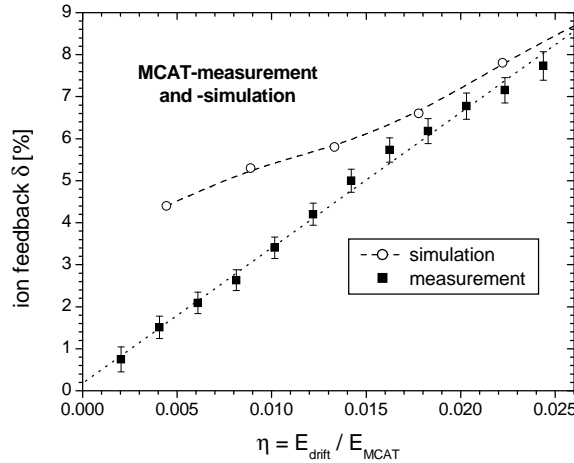


Fig. 5. Comparison of the measured and simulated ion feedback δ as a function of η for the optimised MicroCAT structure.

η . We attribute this effect to attachment of the primary electrons and to recombination with back drifting positive ions. These effects which have not been considered in the simulation seem to be negligible at higher drift fields corresponding to $\eta > 0.02$. We derive an effective electron transparency ε (see Fig. 4) by normalising the measured $\varepsilon \cdot G$ to the simulation of ε at $\eta = 0.02$. The systematic uncertainty of this procedure is indicated in the figure by the enlarged error bars.

We also compare the ion feedback δ with the measurement using the reasonable approximation $G \gg 1$:

$$\delta \approx \frac{I_{\text{drift}} - I_0}{I_{\text{drift}} + I_{\text{MCAT}}} . \quad (6)$$

The measurement deviates considerably from the simulation at small η illustrated in Fig. 5. Obviously, our model is too coarse in this region of η .

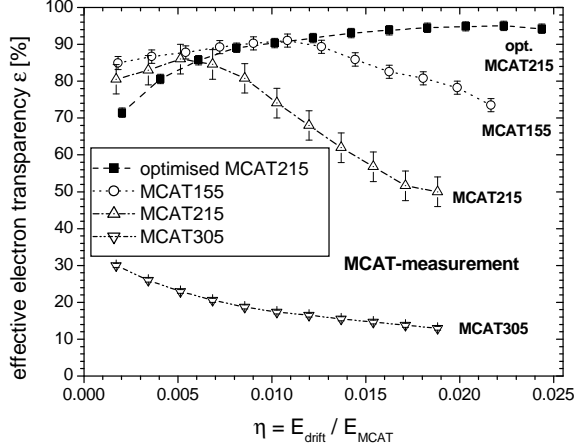


Fig. 6. Comparison of the measured effective electron transparency ε of four MicroCAT structures as a function of η .

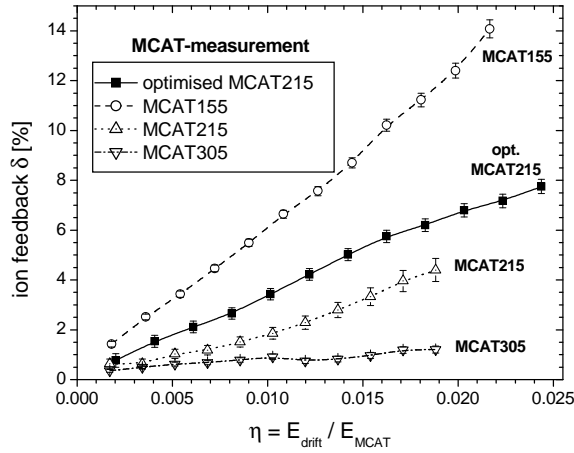


Fig. 7. Comparison of the measured ion feedback δ of four MicroCAT structures as a function of η .

2.2.3 Comparison with other MicroCAT types

Fig. 6 shows a comparison of the measured effective electron transparency ε of four MicroCAT structures with dimensions summarised in Table 1. The optimised mesh offers the largest electron transparency. The drop of the effective electron transparency at low η is different for the different MicroCATs because the amount of gas impurities slightly varies from measurement to measurement.

The comparison of the ion feedback δ of the MicroCAT structures (see Fig. 7) shows, that the fraction of back drifting ions of the optimised MCAT215 structure is nearly as small as for the old MCAT215 structure and lower than that of the MCAT155 device, although the electron transparency ε of the optimised mesh is much larger than that of the competing devices (compare to Fig. 6).

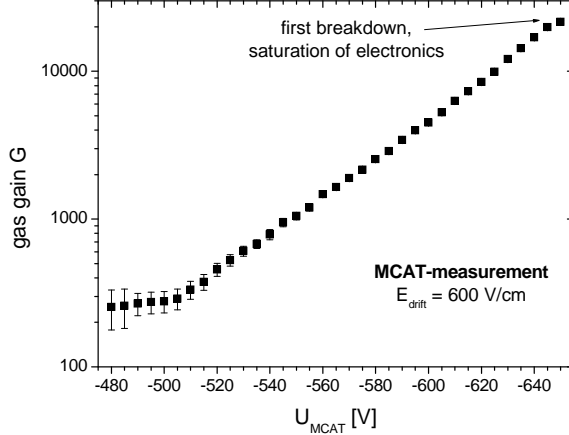


Fig. 8. Measured gas gain G as a function of the applied MCAT voltage.

2.3 Charge multiplication behaviour

Knowing the transparency ε , the gas gain G can be calculated from Eq. 5:

$$G = \frac{I_{\text{drift}} + I_{\text{MCAT}}}{\varepsilon \cdot I_0}. \quad (7)$$

Fig. 8 shows the gain G as a function of the MCAT voltage. It has been obtained from the observed pulse heights of an ^{55}Fe -source where the gain had been calibrated at one voltage to the current measurement. The maximum gain, which we define as the gas amplification, that can be reached within a discharge limit of less than 1 spark/30s, is in the order of $2 \cdot 10^4$.

2.4 Conclusion

The comparison of the optimised and the three previously investigated Micro-CAT structures shows that the new mesh is superior with respect to electron transparency. The ion feedback of the optimised structure is in a reasonable range ($< 8\%$ up to $\eta = 0.025$). In order to reach maximum effective gain the optimised device should be operated with ratios $\eta \approx 0.02$ of the fields above and below the MCAT. A maximum gain of about $2 \cdot 10^4$ can be obtained at atmospheric pressure for Argon gas mixtures.

3 Study of the GEM

The charge transfer and gas gain behaviour of the GEM is investigated by simulations and current measurements to obtain the optimum operation parameters in view of a combination of the GEM with the MicroCAT. The

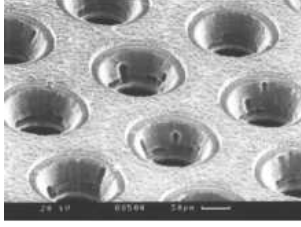


Fig. 9. Scanning electron microscopic photo of the GEM.

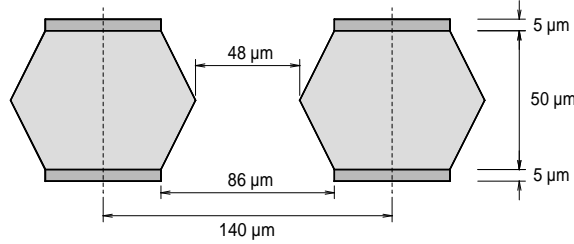


Fig. 10. Vertical cut through the GEM with the dimensions used for the simulation. influence of different voltage settings and gas mixtures and pressures has been studied.

3.1 Characteristics

The GEM structure is fixed above the MicroCAT at a distance of 2 mm (see Fig. 2). The MicroCAT serves as anode with a slightly positive voltage ($U_{\text{MCAT}} \approx +5 \text{ V}$). In this geometry the drift region above the GEM amounts to about 25 mm, the region below the gas electron multiplier corresponds to the distance to the MicroCAT structure, consequently 2 mm. We denote the electric field above and below the GEM with drift field and transfer field, respectively.

The GEM [21] (see Fig. 9), itself, has a hexagonal hole arrangement with a pitch of $140 \mu\text{m}$, an optical transparency of about 12 % and a total thickness of $60 \mu\text{m}$ (see Fig. 10).

The current measurements have been carried out with a ^{55}Fe -source, collimated to 5 mm^2 , emitting photons with a rate of about 45 kHz.

3.2 Charge transfer behaviour

The charge transfer behaviour of the GEM can be described by four current equations. Two electron transparencies are introduced: ε_1 is the probability, that the electrons, coming from the drift/conversion region, reach the centre of a GEM hole; ε_2 is the probability, that these electrons reach the anode. This approach has already been introduced by other groups (see for example

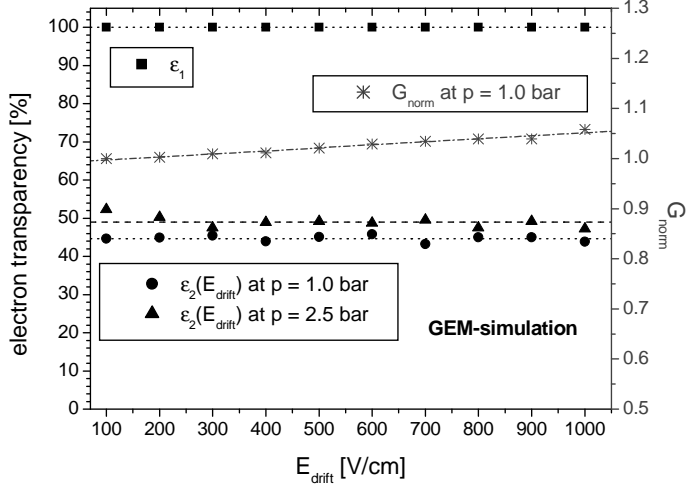


Fig. 11. Simulated electron transparencies ε_1 and ε_2 and normalised gain as a function of the drift field.

in Ref. [22]). The ion feedback is again denoted by δ .

$$I_{\text{drift}} = I_0 + \delta \cdot \varepsilon_1 \cdot (G - 1) \cdot I_0 \quad (8)$$

$$I_{\text{GEM-top}} = -(1 - \varepsilon_1) \cdot I_0 + (1 - \delta) \cdot \varepsilon_1 \cdot (G - 1) \cdot I_0 \quad (9)$$

$$I_{\text{GEM-bottom}} = -\varepsilon_1 \cdot (1 - \varepsilon_2) \cdot G \cdot I_0 \quad (10)$$

$$I_{\text{anode}} = -\varepsilon_1 \cdot \varepsilon_2 \cdot G \cdot I_0 \quad (11)$$

Current conservation reduces these equations to three independent relations. In the following we make use of the effective gain which is defined by $G_{\text{eff}} = \varepsilon_1 \cdot \varepsilon_2 \cdot G$.

3.2.1 Simulations

Like in the previous section the three-dimensional electric field in the GEM geometry and the charge transfer behaviour have been investigated with Maxwell and Garfield, respectively. For the transparency simulation the charge multiplication process has not been considered; ion feedback simulations have not been carried out.

If not stated differently, we have assumed in the simulations a drift field of $E_{\text{drift}} = 500$ V/cm, a transfer field of $E_{\text{trans}} = 2000$ V/cm, a GEM voltage of $\Delta U_{\text{GEM}} = 450$ V and a gas mixture of 1 bar and 2.5 bar Ar/CO₂ (90/10).

3.2.1.1 Influence of the drift field: The dependency of the electron transparencies ε_1 and ε_2 on the applied drift field ($100 \text{ V/cm} \leq E_{\text{drift}} \leq 1000 \text{ V/cm}$) is shown in Fig. 11. All electrons reach the centre of the hole in the GEM structure ($\varepsilon_1 = 1$), independent of the chosen gas pressure. The parameter ε_2 is not influenced noticeably by the drift field. The deviation of

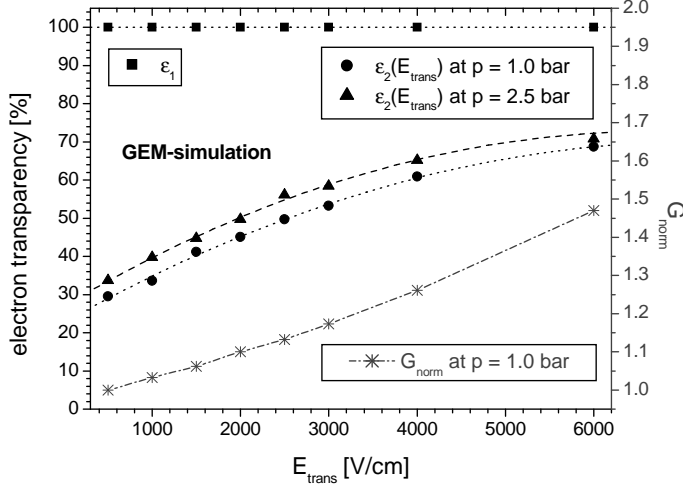


Fig. 12. Simulated electron transparencies ϵ_1 and ϵ_2 and normalised gain as a function of the transfer field.

ϵ_2 between the two gas pressures can be explained by the smaller electron diffusion at higher pressure.

The situation is very different from that in particle physics applications where usually due to rather high drift fields ϵ_1 is smaller than 100%. In our case the overall electron transparency is obviously limited by diffusion effects which cause a large fraction of electrons to be caught by the lower electrode.

We have also studied the effect of drift field variations on the gain G . The gain was calculated with Garfield for one electron starting $100 \mu\text{m}$ above the GEM along the symmetry axis of a hole. The smallest gain $G_{\text{norm}}(E_{\text{drift}})$, which is obtained at a drift field of $E_{\text{drift}} = 100 \text{ V/cm}$, is normalised to 1. The gain increases by about 5% in the investigated drift field range.

3.2.1.2 Influence of the transfer field: The electron transparencies ϵ_1 and ϵ_2 as a function of the applied transfer field ($500 \text{ V/cm} \leq E_{\text{trans}} \leq 6000 \text{ V/cm}$) are shown in Fig. 12. The transparency ϵ_1 is constant $\approx 100\%$ for all applied transfer fields, whereas ϵ_2 shows a strong increase with rising transfer fields. Smaller electron diffusion at higher pressure leads to a larger ϵ_2 . Fig. 12 also shows the normalised gain G_{norm} as a function of the transfer field. The change at low transfer fields is about $5\%/(1000 \text{ V/cm})$; identical as observed with a variation of the drift field (see Fig. 11). At transfer fields $E_{\text{trans}} \gtrsim 4000 \text{ V/cm}$ the parallel plate amplification starts in the gap between the GEM and the anode plane, resulting in an additional contribution to the gain G .

3.2.1.3 Influence of the GEM voltage: The dependence of the electron transparencies on the applied GEM voltage ($50 \text{ V} \leq \Delta U_{\text{GEM}} \leq 500 \text{ V}$) has been studied (see Fig. 13). The transparencies ϵ_1 and ϵ_2 depend only weakly

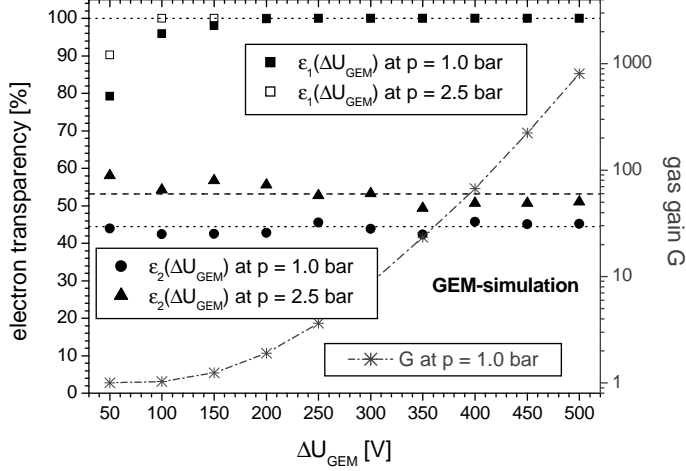


Fig. 13. Simulated electron transparencies ε_1 and ε_2 and gas gain as a function of the GEM voltage.

on the GEM voltage. For very low GEM voltages ε_1 decreases because the drift channel through the GEM holes becomes wider. Smaller diffusion at a gas pressure of 2.5 bar results in a larger electron transparency than for atmospheric pressure. The calculated GEM gain G has the typical exponential shape with increasing operation voltage.

3.2.2 Measurements and comparison with simulations

A gas mixture of Ar/CO₂ (90/10) at a pressure of 1 bar was chosen for most of the measurements if not stated differently. In addition, the charge transfer and multiplication behaviour was investigated for several Argon, Krypton, Xenon and CO₂-quench gas mixtures at various pressures up to 2.5 bar. From Eqs. 8–11 the product $\varepsilon_1 \cdot G$, the transparency ε_2 and the ion feedback δ (using the reasonable approximation $G \gg 1$) can be calculated:

$$\varepsilon_1 \cdot G = -\frac{(I_{\text{GEM-bottom}} + I_{\text{anode}})}{I_0} \quad (12)$$

$$\varepsilon_2 = \frac{I_{\text{anode}}}{I_{\text{GEM-bottom}} + I_{\text{anode}}} \quad (13)$$

$$\delta \approx \frac{I_{\text{drift}} - I_0}{I_{\text{drift}} + I_{\text{GEM-top}}} \quad (14)$$

3.2.2.1 Influence of the drift field: Fig. 14 shows the influence of the drift field on the product $\varepsilon_1 \cdot G$ for various gas pressures of Kr/CO₂ (90/10). The decrease at small drift fields is again attributed to recombination and

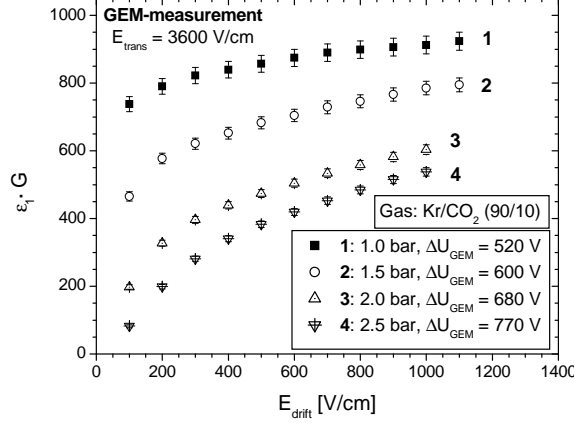


Fig. 14. Measured product $\varepsilon_1 \cdot G$ as a function of the drift field for several gas pressures of Kr/CO₂ (90/10).

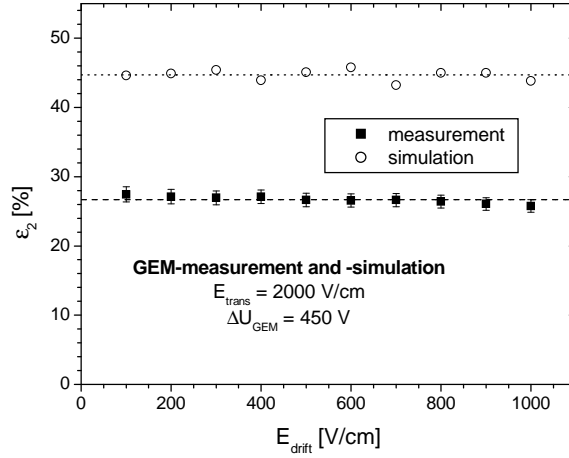


Fig. 15. Comparison between the measured and the simulated electron transparency ε_2 as a function of the drift field.

attachment effects which are expected to increase with gas pressure. The simulation (see Fig. 11) indicates that the gain G slightly depends on the drift field, whereas the transparency $\varepsilon_1 = 1$ is constant. Therefore the measured electron transparency ε_1 can be assumed to be very close to 100 %.

The measurements show that the transparency ε_2 does not change noticeably with the varying drift field (see Fig. 15). This is in line with expectation and simulation. However, the transparency ε_2 is apparently overestimated in the simulation, which means that in reality more electrons move to the GEM-bottom electrode. Possible explanations of this effect could be:

- (1) neglect of the avalanche development in the simulation: repulsive forces and UV-photons widen the electron cloud.
- (2) underestimation of the electron diffusion at high electric fields in Magboltz.

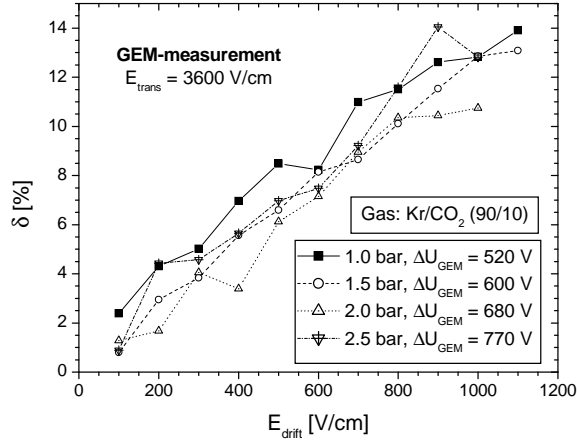


Fig. 16. Measured ion feedback δ as a function of the drift field at different gas pressures of Kr/CO₂ (90/10).

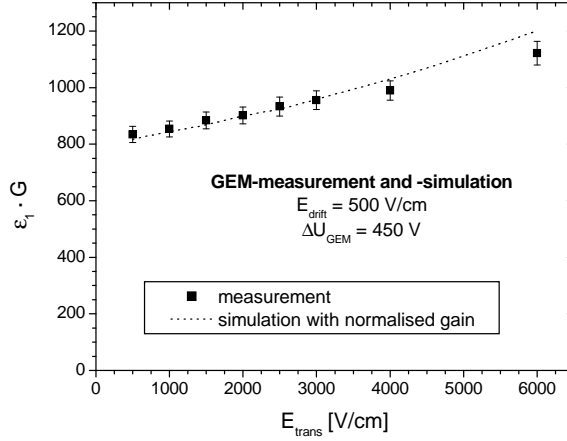


Fig. 17. Comparison between the measured and the simulated product $\epsilon_1 \cdot G$ as a function of the transfer field.

The measured ion feedback δ of the GEM is presented in Fig. 16 for several gas pressures of Kr/CO₂ (90/10). It increases nearly linearly with rising drift field.

3.2.2.2 Influence of the transfer field: The measured increase of $\epsilon_1 \cdot G$ with rising E_{trans} (see Fig. 17) is in a good agreement with the increase of the gain G which was predicted by the simulation (compare to Fig. 12). Thereby the simulated gain had to be renormalised because of the inaccurate knowledge of the corresponding Townsend coefficients. We conclude that ϵ_1 is not sizeably influenced by the transfer field.

However, the transparency ϵ_2 increases strongly with rising transfer fields (see Fig. 18). The deviation of the absolute values of ϵ_2 between simulation and measurement has already been discussed in section 3.2.2.1. For transfer fields

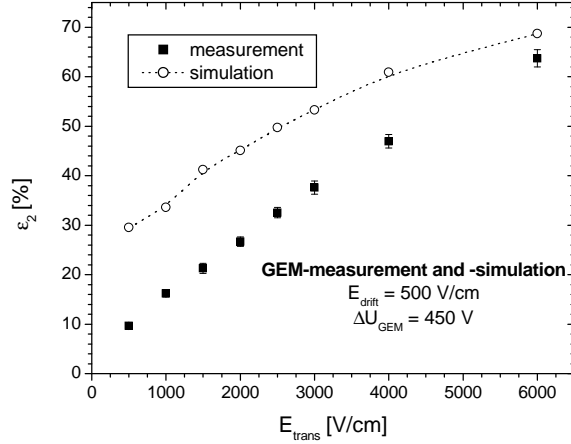


Fig. 18. Comparison between the measured and the simulated transparency ε_2 as a function of the transfer field.

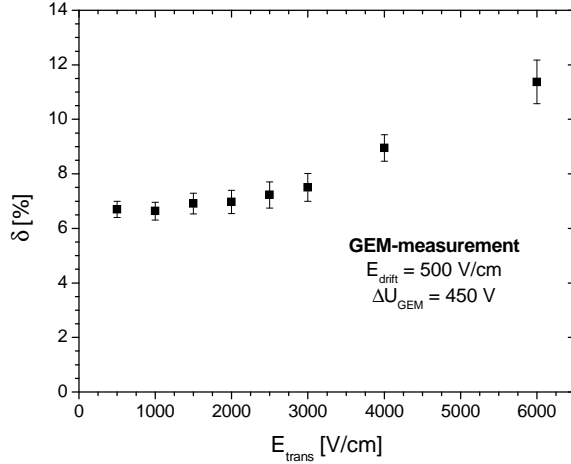


Fig. 19. Measured ion feedback δ as a function of the transfer field.

$E_{\text{trans}} \gtrsim 4000$ V/cm the parallel plate amplification underneath the GEM leads to an apparent rise of ε_2 which is more pronounced in the measurement due to the longer multiplication path of 2 mm compared to $100 \mu\text{m}$ in the simulation. The measured ion feedback δ (see Fig. 19) is approximately constant at lower transfer fields. When the parallel plate amplification produces a noticeable amount of gain (at large transfer fields) the ion feedback rises. We conclude that the ion feedback is larger for ions which are produced below the GEM rather than in the GEM holes.

3.2.2.3 Influence of the GEM voltage: The expected exponential dependence of $\varepsilon_1 \cdot G$ on the GEM voltage is shown in Fig. 20 for Ar/CO₂ (70/30) at various gas pressures.

With increasing ΔU_{GEM} the transparency ε_2 decreases (see Fig. 21). For high

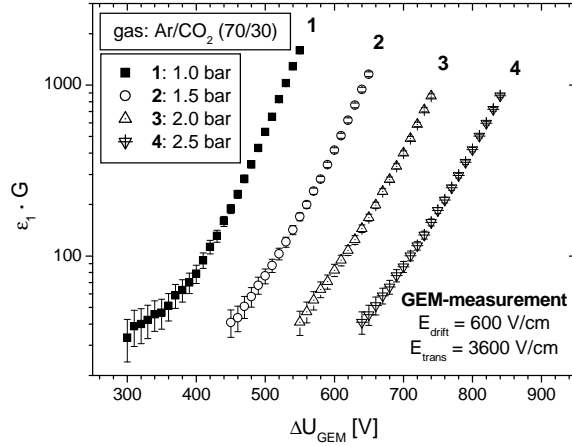


Fig. 20. Measured product $\varepsilon_1 \cdot G$ as a function of the GEM voltage in Ar/CO₂ (70/30) at several gas pressures.

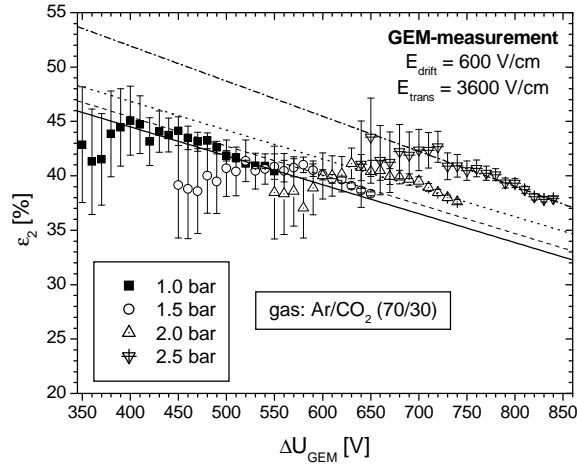


Fig. 21. Measured electron transparency ε_2 as a function of the GEM voltage in Ar/CO₂ (70/30) at several gas pressures.

GEM fields the electron drift channel becomes very narrow. As a consequence the probability that electrons diffuse to one of the dense drift lines that end on the GEM bottom electrode is increased.

The ion feedback as a function of the GEM voltage is shown in Fig. 22. Due to very small currents at the drift cathode at low gains the error bars are very large. The deviations from a constant behaviour are not significant.

3.3 Charge multiplication behaviour

We have investigated the gain behaviour of the GEM for different gas mixtures and pressures. The maximum gas amplification, which can be reached within a

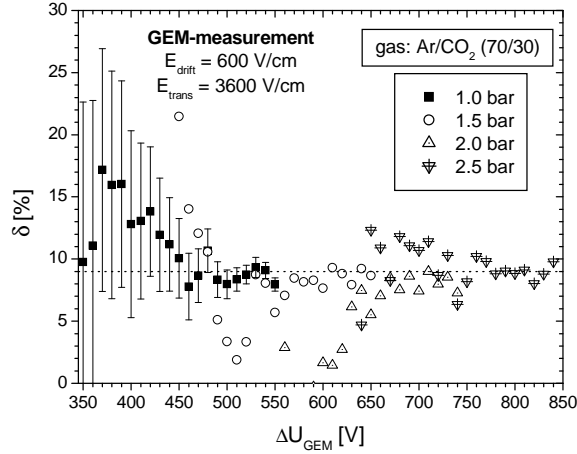


Fig. 22. Measured ion feedback δ as a function of the GEM voltage in Ar/CO₂ (70/30) at several gas pressures.

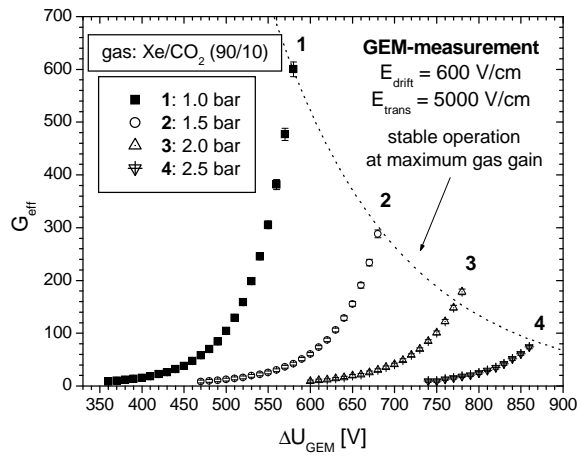


Fig. 23. Measured effective gain $G_{\text{eff}} = \varepsilon_1 \varepsilon_2 G$ as a function of the GEM voltage in Xe/CO₂ (90/10) at several gas pressures.

discharge limit of less than 1 spark/30 s, decreases drastically with gas pressure (shown as an example for a Xe/CO₂ (90/10) gas mixture in Fig. 23). This effect is studied in more detail in Ref. [23].

3.4 Conclusion

The approach of the introduction of the two electron transparencies ε_1 and ε_2 has been sensibly confirmed by our measurements.

The systematic studies of the currents at the electrodes in a wide range of voltages and electric fields show the following results:

- The transparencies ε_1 and ε_2 do not depend significantly on the drift field for $E_{\text{drift}} \lesssim 1$ kV/cm. The ion feedback δ rises nearly linearly with increasing drift field. In order to avoid electron losses due to recombination and attachment in the conversion region the drift field should not be chosen too small, especially for higher gas pressures. The gain G rises slightly with increasing drift field.
- The transfer field has no influence on the electron transparency ε_1 in the investigated field range $E_{\text{trans}} \lesssim 6$ kV/cm. The transparency ε_2 strongly rises with increasing transfer fields. The ion feedback δ does not change noticeably for small transfer fields and increases slightly for higher transfer fields. Also the gain G rises with increasing transfer field.
- Very small GEM voltages lead to a decrease of ε_1 . The transparency ε_2 decreases slightly for large potential differences, whereas the ion feedback δ is nearly constant.

4 The combination of the optimised MicroCAT with the GEM

The combination of the optimised MCAT215 and the GEM has been investigated by current measurements to determine the optimum voltage settings with respect to maximum effective gain and minimum ion feedback. The maximum gas gain in different gas environments has been studied. No simulations have been carried out. However, the results of the individual simulations from Sections 2 and 3 can be combined.

4.1 Characteristics

Fig. 2 shows the schematic setup of the combination of MicroCAT and GEM. We call the electric field between the drift cathode and the GEM by E_{drift} , the field between the GEM and the MCAT by E_{trans} and between the MCAT and the anode by $E_{\text{MCAT}} \equiv U_{\text{MCAT}}/d$, where U_{MCAT} denotes the voltage applied to the MCAT and $d = 130 \mu\text{m}$ the distance between MCAT and anode. The ratio of the fields above and below the MicroCAT structure is denoted by $\eta = E_{\text{trans}}/E_{\text{MCAT}}$. The electron transparency, ion feedback and gain of the MicroCAT are denoted by $\varepsilon_{\text{MCAT}}$, δ_{MCAT} and G_{MCAT} , respectively. All GEM transparencies are denoted as in the previous section, the GEM gain is denoted by G_{GEM} . The total effective gain is defined as follows:

$$G_{\text{eff}} = \varepsilon_1 \cdot \varepsilon_2 \cdot \varepsilon_{\text{MCAT}} \cdot G_{\text{GEM}} \cdot G_{\text{MCAT}} \quad (15)$$

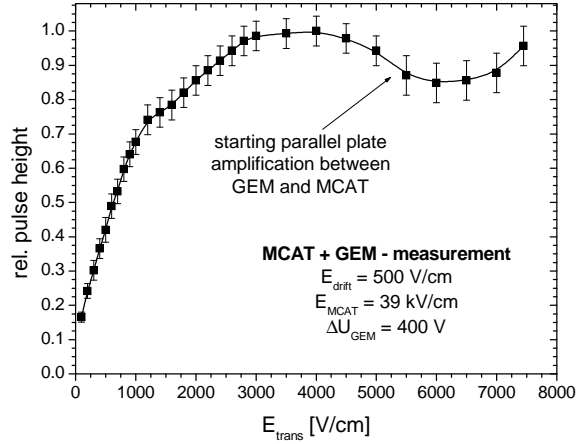


Fig. 24. Measured relative pulse height as a function of the transfer field E_{trans} for the combination of MCAT and GEM.

4.2 Charge transfer behaviour

Fig. 24 shows the relative signal pulse heights as a function of the transfer field for a drift field of $E_{\text{drift}} = 500 \text{ V/cm}$, a GEM voltage of $\Delta U_{\text{GEM}} = 400 \text{ V}$, an MCAT voltage of $U_{\text{MCAT}} = -510 \text{ V}$ at a gas pressure of 1 bar Ar/CO₂ (90/10). Up to transfer fields of $E_{\text{trans}} \approx 3000 \text{ V/cm}$ the signal pulse height rises. The subsequent plateau reaches up to $E_{\text{trans}} \approx 4000 \text{ V/cm}$, before the signals get smaller again. At very high transfer fields of $E_{\text{trans}} \gtrsim 5000 \text{ V/cm}$ parallel plate amplification between GEM and MicroCAT starts, which again leads to an increase of the signals' pulse heights.

The shape of this curve is affected by two opposite effects: on the one hand the transparency ε_2 of the GEM rises for increasing transfer fields (compare to Fig. 18), and on the other hand the electron transparency $\varepsilon_{\text{MCAT}}$ of the MicroCAT drops for larger values of η (compare to Fig. 3). With the knowledge of $\varepsilon_2(E_{\text{trans}})$, determined in section 3, the electron transparency of the MCAT can be calculated up to values of $\eta \approx 0.2$. The result is shown in Fig. 25. It agrees perfectly with the transparency measured directly with the MicroCAT alone (see Fig. 4). Measurements at different GEM voltages show the same results. However, a large deviation from the simulation is obvious for $\eta \gtrsim 0.04$. The measured transparency $\varepsilon_{\text{MCAT}}$ is significantly smaller than what the simulation predicts. We have no explanation for this effect.

By means of current relations and the reasonable assumptions, that $\varepsilon_1 = 1$, $G_{\text{GEM}} \gg 1$ and $G_{\text{MCAT}} \gg 1$ the ion feedback δ_{MCAT} of the MicroCAT can be determined:

$$\delta_{\text{MCAT}} \approx 1 - \frac{I_{\text{MCAT}}}{G_{\text{eff}} \cdot I_0} - (1 - \varepsilon_{\text{MCAT}}) \cdot \varepsilon_2 \cdot \frac{G_{\text{GEM}}}{G_{\text{eff}}}$$

The result (see Fig. 26) shows a good agreement to the direct measurement

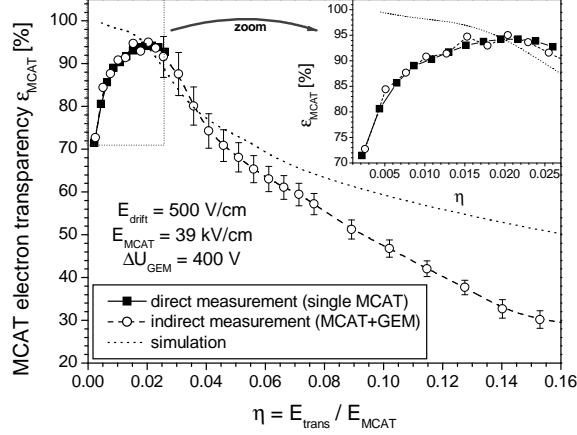


Fig. 25. Comparison between the directly and indirectly determined electron transparency $\varepsilon_{\text{MCAT}}$ as a function of η for constant E_{MCAT} . In addition the simulated electron transparency is shown.

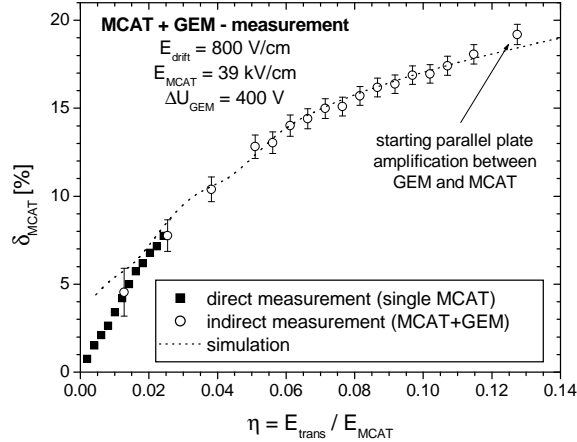


Fig. 26. Comparison between the directly and indirectly determined ion feedback δ_{MCAT} as a function of η for constant E_{MCAT} . In addition the simulated ion feedback is shown.

(compare to Fig. 5). Despite the coarse model for the ion feedback simulation the simulation and the measurement match very well for larger ratios η . Additional measurements have shown that the field in the conversion region $E_{\text{drift}} \lesssim 1 \text{ kV/cm}$ above the GEM has no influence on the ion feedback δ_{MCAT} . Fig. 27 shows, that the total ion feedback $\delta = -I_{\text{drift}}/I_{\text{anode}}$ is getting more favourable for higher transfer fields. The GEM voltage has no strong effect on the total ion feedback δ (see Fig. 28). The increase of the total ion feedback δ with decreasing MCAT voltage (see Fig. 29) can be explained by the rising contribution of the ion feedback δ_{MCAT} , which gets larger for higher ratios $\eta = E_{\text{trans}}/E_{\text{MCAT}}$ (compare to Fig. 26).

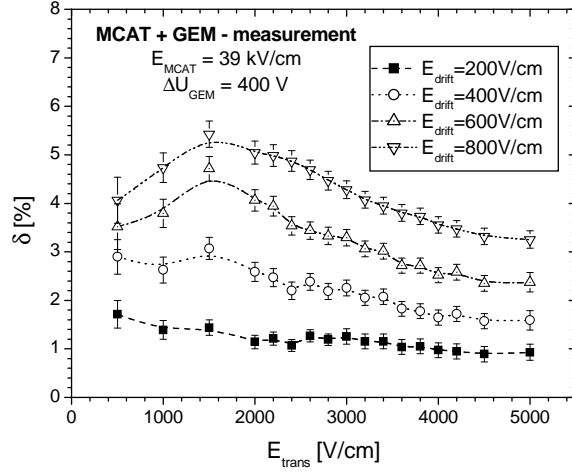


Fig. 27. Measured total ion feedback δ as a function of the transfer field E_{trans} .

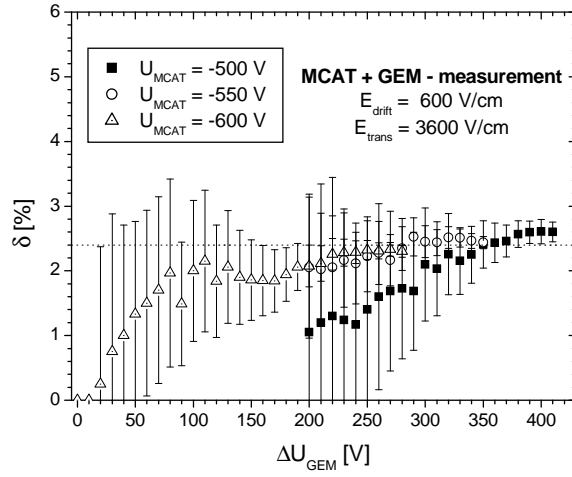


Fig. 28. Measured total ion feedback δ as a function of the GEM voltage ΔU_{GEM} .

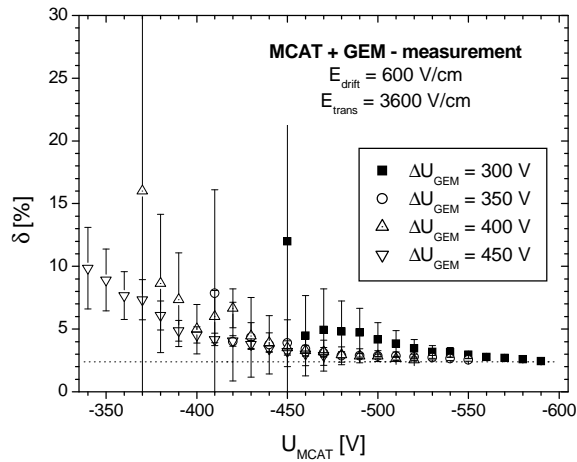


Fig. 29. Measured total ion feedback δ as a function of the MCAT voltage U_{MCAT} .

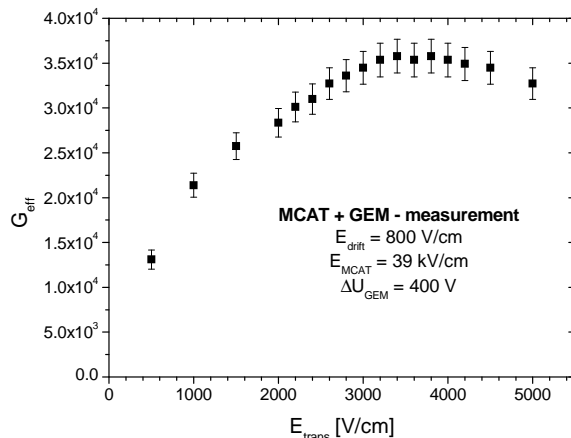


Fig. 30. Measured effective gain G_{eff} as a function of the transfer field E_{trans} .

4.3 Charge multiplication behaviour

The effective gain G_{eff} (see Eq. 15) of the GEM/MicroCAT-combination can be calculated from the measured currents I_0 (see Eq. 4) and I_{anode} as follows:

$$G_{\text{eff}} = -\frac{I_{\text{anode}}}{I_0}$$

The effective gain as a function of the transfer field rises to maximum at $E_{\text{trans}} \approx 3.6 \text{ kV/cm}$ in 1 bar Ar/CO₂ (90/10) (see Fig. 30).

In order to study the maximum gas gain a systematic investigation of the effective gain G_{eff} as a function of the gas pressure has been carried out for different noble gas/quench gas mixtures. The GEM voltages are chosen such, that this fragile pre-amplification device always works in a safe range, whereas the MCAT produces the main amplification. This method has the advantage that all discharges appear below the MicroCAT structure, which is not easily damaged by sparks. All sparks appear at a defined avalanche size depending on the gas mixture and pressure used, but independent on the voltage settings on GEM or on MCAT.

The measurements of the maximum gas gain are carried out for gas pressures up to 2.5 bar. Fig. 31 shows the measured maximum gain for several pressures of Kr/CO₂ (90/10) and Xe/CO₂ (90/10). In a first approximation the drop of the gain for higher pressures is approximately exponential. The results of the exponentially fitted data are shown in Fig. 32. The largest gas gain of about $2 \cdot 10^5$ can be achieved with the gas mixture of Ar/CO₂ (90/10). At atmospheric pressure the gain decreases with the atomic number of the noble gas. We estimate that for gas pressures up to 4 bar gains of at least $G_{\text{eff,max}} > 2 \cdot 10^3$ can be reached, even for Xe-mixtures.

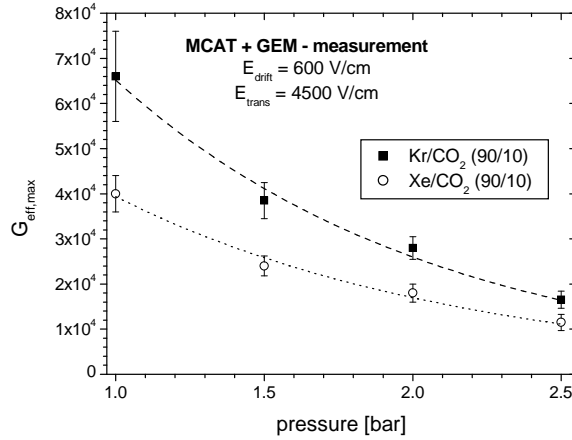


Fig. 31. Maximum gas gain $G_{\text{eff,max}}$ as a function of the pressure for a Kr/CO₂ (90/10) and a Xe/CO₂ (90/10) gas mixture. The lines correspond to exponential fits of the measured data.

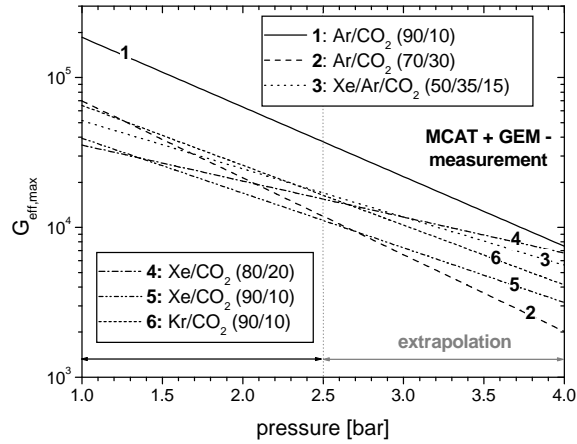


Fig. 32. Maximum gas gain $G_{\text{eff,max}}$ as a function of the pressure for six different gas mixtures. The curves correspond to exponential fits of the measured data and are extrapolated up to pressures of 4 bar.

4.4 Conclusion

The investigation of the optimum voltage settings for a GEM/MicroCAT-combination leads to the following results:

- To avoid recombination and attachment effects the drift field above the GEM should be chosen larger than 500 V/cm. Higher gas pressure requires larger drift fields (compare to Section 3 and Fig. 14).
- A transfer field in the range of 3000 – 4000 V/cm ensures a maximum effective gain and a small total ion feedback.

- Since the combined gain of the GEM and the MicroCAT is limited and because the GEM is easily destroyed by discharges the MicroCAT should be operated at much higher gain than the GEM.

The maximum gas gain decreases with pressure and atomic number of the noble gas. A stable operation with gains in the order of 10^4 can be obtained even for Xenon gas mixtures up to 2.5 bar.

5 Conclusion

The new optimised MicroCAT structure is superior to all other MicroCAT devices with respect to electron transparency. The ion feedback of the new mesh is smaller than for the MCAT155 and nearly as good as for the old MCAT215 structure. Gas gains of larger than $2 \cdot 10^4$ can be achieved in Argon gas mixtures at standard pressure.

In our special detector setup a GEM has been investigated with respect to its charge transfer and gas gain behaviour with different voltage settings and different gas environments. The charge transfer simulations are well confirmed by the measurements. A sub-division of the overall electron transparency into the two transparencies ε_1 and ε_2 is reasonable. The achieved gains of the GEM are comparable to published results.

The combination of both gas gain devices leads to a very high gas gain at atmospheric pressure and a reliable detector operation with gains in the order of 10^4 in Xenon gas mixtures at higher pressures of about 2.5 bar. The GEM can be operated in a very safe gas gain mode, whereas the the MicroCAT produces the largest amount of gain; due to the robustness of the nickel mesh and its insensitivity against sparking no destruction of this device needs to be feared. The fraction of back drifting ions is in the order of a few percent when MicroCAT and GEM are combined. Therefore, spatial reconstruction distortions due to space charge effects in the conversion region are expected to be small.

Acknowledgements

We are indebted to G. Claassen and T. van de Mortel from Stork Screens. Only due to their effort the prototype production of the optimised MicroCAT mesh was possible. We are grateful to G. Zech for valuable comments that have contributed to this publication.

References

- [1] F. Sauli. *GEM: A new concept for electron amplification in gas detectors*, Nucl. Instr. and Meth. **A 386** (1997) 531
- [2] Y. Giomataris, Ph. Rebourgeard, J.P. Robert, G. Charpak. *MICROMEGAS: A high-granularity position-sensitive gaseous detector for high particle-flux environments*, Nucl. Instr. and Meth. **A 376** (1996) 29
- [3] F. Bartol, M. Bordessoule, G. Chaplier, M. Lemonnier, S. Megtert. *The C.A.T. Pixel Proportional Gas Counter Detector*, J. Phys. III France **6** (1996) 337
- [4] A. Sarvestani, H.J. Besch, M. Junk, W. Meissner, N. Sauer, R. Stiehler, A.H. Walenta, R.H. Menk. *Study and application of hole structures as gas gain devices for two dimensional high rate X-ray detectors*, Nucl. Instr. and Meth. **A 410** (1998) 238
- [5] Y. Benhammou, J.M. Brom, J.C. Fontaine, D. Huss, F. Jeanneau, A. Lounis, I. Ripp-Baudot, A. Zghiche. *Comparative studies of MSGC and MSGC-GEM detectors*, Nucl. Instr. and Meth. **A 419** (1998) 400
- [6] O. Baruth, S. Keller, U. Werthenbach, G. Zech, T. Zeuner. *Sparks in MSGC and GEM detectors and a robust alternative*, Nucl. Instr. and Meth. **A 454** (2000) 272
- [7] Y. Bagaturia, O. Baruth, H.B. Dreis, F. Eisele, I. Gorbunov, S. Gradl, W. Gradl, S. Hausmann, M. Hildebrandt, T. Hott, S. Keller, C. Krauss, B. Lomonosov, M. Negodaev, C. Richter, P. Robmann, B. Schmidt, U. Straumann, P. Truöl, S. Visbeck, T. Walter, C. Werner, U. Werthenbach, G. Zech, T. Zeuner, M. Ziegler. *Studies of aging and HV break down problems during development and operation of MSGC and GEM detectors for the Inner Tracking System of HERA-B*, accepted for publication in Nucl. Instr. and Meth.
- [8] P. Fonte, V. Peskov, B.D. Ramsey. *Rate and gain limitations of MSGCs and MGCs combined with GEM and other preamplification structures*, Nucl. Instr. and Meth. **A 419** (1998) 405
- [9] I. Reichwein, U. Werthenbach, G. Zech. *Properties of Groove Chambers*, accepted for publication in Nucl. Instr. and Meth.
- [10] S. Kane, J. May, J. Miyamoto, I. Shipsey. *A study of micromegas with preamplification with a single GEM*, Proceeding for the International conference on advanced technology and particle physics, Villa Olmo, Como, Italy, Oct 15-19 (2001), submitted to World Scientific (2002)
- [11] S. Bachmann, A. Bressan, L. Ropelewski, F. Sauli, A. Sharma, D. Mörmann. *Charge amplification and transfer processes in the gas electron multiplier*, Nucl. Instr. and Meth. **A 438** (1999) 376
- [12] A. Buzulutskov, A. Breskin, R. Chechik, G. Garty, F. Sauli, L Shekhtman. *The GEM photomultiplier operated with noble gas mixtures*, Nucl. Instr. and Meth. **A 443** (2000) 164

- [13] A. Buzulutskov, A. Breskin, R. Chechik, G. Garty, F. Sauli, L. Shekhtman. *Further studies of the GEM photomultiplier*, Nucl. Instr. and Meth. **A 442** (2000) 68
- [14] A. Orthen, H. Wagner, H.J. Besch, R.H. Menk, A.H. Walenta. *Charge transfer considerations of MicroCAT-based detector systems*, Nucl. Instr. and Meth. **A 492** (2002) 160
- [15] H.J. Besch, M. Junk, W. Meissner, A. Sarvestani, R. Stiehler, A.H. Walenta. *An interpolating 2D pixel readout structure for synchrotron X-ray diffraction in protein crystallography*, Nucl. Instr. and Meth. **A 392** (1997) 244
- [16] H. Wagner, H.J. Besch, R.H. Menk, A. Orthen, A. Sarvestani, A.H. Walenta, H. Walliser. *On the dynamic two-dimensional charge diffusion of the interpolating readout structure employed in the MicroCAT detector*, Nucl. Instr. and Meth. **A 482** (2002) 334
- [17] Maxwell 3D Field Simulator Version 5.0.04, Ansoft Corporation, Pittsburgh, PA USA
- [18] Garfield, CERN Wire Chamber Field and Transport Computation Program written by R. Veenhof, Version 7.05 (2001)
- [19] S.F. Biagi. *Monte Carlo simulation of electron drift and diffusion in counting gases under the influence of electric and magnetic fields*, Nucl. Instr. and Meth. **A 421** (1999) 234
- [20] Magboltz, CERN Transport of Electrons in Gas Mixtures Computation Program written by S.F. Biagi, Version 2
- [21] J. Benlloch, A. Bressan, C. Buttner, M. Capeans, M. Gruwe, M. Hoch, J.-C. Labbé, A. Placci, L. Ropelewski, F. Sauli, A. Sharma, R. Veenhof. *Development of the gas electron multiplier (GEM)*, IEEE Trans. Nucl. Sci. **45** (1998) 234-243
- [22] C. Richter, A. Breskin, R. Chechik, D. Mörmann, G. Garty, A. Sharma. *On the efficient electron transfer through GEM*, Nucl. Instr. and Meth. **A 478** (2002) 528
- [23] A. Bondar, A. Buzulutskov, F. Sauli, L. Shekhtman. *High- and low-pressure operation of the gas electron multiplier*, Nucl. Instr. and Meth. **A 419** (1998) 418